Calculation of Transonic Internal Flows Using an Efficient High Resolution Upwind Scheme

Ge-Cheng Zha*and Zongjun Hu†
Dept. of Mechanical Engineering
University of Miami
Coral Gables, Florida 33124
E-mail: zha@apollo.eng.miami.edu

Abstract

A new efficient upwind scheme based on the concept of convective upwind and split pressure (CUSP) is developed. The upwinding of the convective term and the pressure split are consistent with their characteristic directions. The scheme has low diffusion to accurately resolve wall boundary layers, and are able to capture crisp shock waves and exact contact discontinuities. The accuracy of the scheme is compared with other popularly used schemes including Roe scheme, Liou's AUSM$^+$ scheme, Van Leer scheme, and Van Leer-Hänel scheme. The scheme is tested for the 1D Sod shock tube problem, 1D slowly moving contact surface, supersonic flat plate laminar boundary layer, a transonic nozzle with oblique shock waves and reflections that do not align with the mesh lines, and a transonic inlet diffuser with shock wave/turbulent boundary layer interaction. The test cases show that the new scheme is accurate, robust and efficient.

1 Introduction

Development of an accurate and efficient numerical scheme for compressible flow governing equations is essential due to the increasing engineering demand for aircraft and spacecraft design[1]. Such a scheme is particularly important when aircraft engine turbomachinery aeroelasticity problems are simulated using a fully coupled fluid/structural model, which is usually very CPU intensive. Hence an accurate, efficient and robust upwind scheme used as the Riemann solver to resolve shock waves, contact surface discontinuities and wall boundary layers is very desirable.

To achieve the purpose of efficiency and accuracy, efforts have been made to develop upwind schemes only using scalar dissipation instead of matrix dissipation such as that of the Roe's flux difference splitting (FDS) scheme [2]. The examples include AUSM family schemes of Liou represented by their latest scheme of AUSM$^+$[3, 4, 5, 6, 7], the Van Leer-Hänel scheme[8], Edwards's LDFSS schemes[9, 10], Jameson's CUSP schemes and limiters[11, 12, 13], and the schemes developed by Zha, et al.[14, 15, 16], etc.

Pioneered by Liou and Steffen[3, 5, 6], the researchers seeking the scalar dissipation primarily follow the guideline that the velocity and pressure should be separated to consider their characteristics representing the physics of the convection and waves. Liou and his colleagues termed their schemes as advection upstream splitting method(AUSM) schemes, and Jameson gave the name of convective upwind and split pressure (CUSP) schemes[11, 12, 13]. The name of CUSP seems more precisely reflecting the physical meaning.

As pointed out by Jameson[11, 12, 13], the CUSP schemes can be basically categorized to two types, the H-CUSP and E-CUSP. The H-CUSP schemes has the total enthalpy from the energy equation in their convective vector, while the E-CUSP schemes use the total energy in the convective vector. The Liou's AUSM family schemes, Van Leer-Hänel scheme[8], and Edwards's LDFSS schemes[9, 10] belong to the H-CUSP group. The H-CUSP schemes may have the advantages to better conserve the total enthalpy for steady state flows. The schemes developed by Zha[14, 15] belong to the E-CUSP group. Jameson suggested schemes for both groups[11, 12, 13].

Even though the H-CUSP schemes such as AUSM family schemes have achieved great success, from the characteristic theory point of view, the schemes are not fully consistent with the disturbance propagation directions, which may affect the stability and robustness of the schemes. By splitting the eigenvalues of the Jacobians to convection (velocity) and waves (speed of sound), one will find that the convection terms only contain the total energy[14], which will lead to the E-CUSP schemes. However, the early E-CUSP schemes could not handle contact discontinuities[11, 12, 13, 14]. Borrowing from AUSMDV scheme[4], Zha used the in-

* Associate Professor, AIAA Member
† PhD Student

terface speed of sound and made his E-CUSP scheme able to capture exact contact discontinuities. However, due to lacking the proper numerical dissipation, the scheme will generate odd-even pressure oscillations when applied to multi-dimensional flows.

The purpose of this paper is to develop a high resolution E-CUSP scheme that is consistent with the characteristic directions, and is also accurate, efficient, and robust. The high resolution means that it can accurately resolve the wall boundary shear layers, shock wave and contact discontinuities.

2 The Numerical Scheme

2.1 Governing Equations

To describe the new scheme, we will begin with the quasi-1D Euler equations in Cartesian coordinates for inviscid flow:

$$\partial_t \mathbf{U} + \partial_x \mathbf{E} - \mathbf{H} = 0 \tag{1}$$

where $\mathbf{U} = S\mathbf{Q}$, $\mathbf{Q} = \begin{pmatrix} \rho \\ \rho u \\ \rho e \end{pmatrix}$, $\mathbf{E} = S\mathbf{F}$,

$$\mathbf{F} = \begin{pmatrix} \rho u \\ \rho u^2 + p \\ (\rho e + p)u \end{pmatrix}, \quad \mathbf{H} = \frac{dS}{dx} \begin{pmatrix} 0 \\ p \\ 0 \end{pmatrix} \tag{2}$$

In above equations, ρ is the density, u is the velocity, p is the static pressure, e is the total energy per unit mass and S is the cross sectional area of the 1D duct. The following state equation is also employed:

$$p = (\gamma - 1)(\rho e - \frac{1}{2}\rho u^2) \tag{3}$$

where γ is the specific heat ratio with the value of 1.4 for ideal gas.

The finite volume method with the explicit Euler temporal integration is used to discretize the governing equations. It yields the following formulation at cell i:

$$\Delta \mathbf{Q}_i^{n+1} = \Delta t[-C(\mathbf{E}_{i+\frac{1}{2}} - \mathbf{E}_{i-\frac{1}{2}}) + \frac{\mathbf{H}_i}{S_i}]^n \tag{4}$$

where $C = 1/(\Delta x S_i)$, n is the time level index. A numerical scheme is needed to evaluate the interface flux:

$$\mathbf{E}_{i+\frac{1}{2}} = S\mathbf{F}_{i+\frac{1}{2}} \tag{5}$$

2.2 Characteristics

To develop the scheme for $\mathbf{F}_{i+\frac{1}{2}}$, we need to analyze the characteristics first. It is well known that the eigenvalues of the Jacobian matrix are $u + a, u, u - a$. That is

$$\mathbf{A} = \frac{\partial \mathbf{F}}{\partial \mathbf{Q}} = \mathbf{T}\mathbf{\Lambda}\mathbf{T^{-1}} \tag{6}$$

where $\mathbf{T} = \begin{pmatrix} 1 & 1 & 1 \\ u-a & u & u+a \\ H-ua & \frac{1}{2}u^2 & H+ua \end{pmatrix}$ and

$\mathbf{\Lambda} = \begin{pmatrix} u-a & 0 & 0 \\ 0 & u & 0 \\ 0 & 0 & u+a \end{pmatrix}$.

Due to the homogeneous relationship between $\mathbf{Q}$ and $\mathbf{F}$, we have

$$\mathbf{F} = \mathbf{T}\mathbf{\Lambda}\mathbf{T^{-1}}\mathbf{Q} \tag{7}$$

The Steger-Warming scheme[17] and Roe scheme[2] are directly based on above characteristic relations. For supersonic flows, all the eigenvalues are positive and a numerical scheme can simply take the upwind differencing. The difficulty in constructing a Riemann solver for interface flux $\mathbf{F}$ appears in the subsonic regime, where the acoustic waves propagate in both downstream and upstream directions. To separate the convective terms and wave terms, the eigenvalue matrix may be split as the following[14]:

$$\mathbf{F} = \mathbf{T}\begin{pmatrix} u & 0 & 0 \\ 0 & u & 0 \\ 0 & 0 & u \end{pmatrix}\mathbf{T^{-1}}\mathbf{Q} + \mathbf{T}\begin{pmatrix} -a & 0 & 0 \\ 0 & 0 & 0 \\ 0 & 0 & a \end{pmatrix}\mathbf{T^{-1}}\mathbf{Q}$$

$$= \mathbf{F^c} + \mathbf{F^p} \tag{8}$$

where

$$\mathbf{F^c} = u\begin{pmatrix} \rho \\ \rho u \\ \rho e \end{pmatrix}, \mathbf{F^p} = \begin{pmatrix} 0 \\ p \\ pu \end{pmatrix} \tag{9}$$

Obviously, the vector $\mathbf{F^c}$ has the eigenvalues of velocity and hence is the convective terms. The vector $\mathbf{F^p}$ has the eigenvalues of speed of sound which represents the acoustic waves propagating in each direction at subsonic regime. Above relations will lead to the so called E-CUSP schemes that has the total energy term in the convective vector, $\mathbf{F^c}$.

Based on the above separation of convective and wave terms in subsonic regime, Zha et al.[14, 15, 16] suggested to treat the convective term $\mathbf{F^c}$ in a simple upwind manner and to average the wave term $\mathbf{F^p}$ in

both upwind and downwind direction with the weight of $u \pm a$.

The H-CUSP schemes absorb the pressure term in the energy equation of $\mathbf{F^p}$ into the convective vector in terms of the total enthalpy. The convective vector and wave vector hence become:

$$\mathbf{F'^c} = u \begin{pmatrix} \rho \\ \rho u \\ \rho H \end{pmatrix}, \qquad \mathbf{F'^p} = \begin{pmatrix} 0 \\ p \\ 0 \end{pmatrix} \tag{10}$$

where H is the total enthalpy

$$H = \frac{\rho e + p}{\rho} \tag{11}$$

The eigenvalues of $\mathbf{F'^c}$ are $(u, u, \gamma u)$, and the eigenvalues of $\mathbf{F'^p}$ are $[0, 0, -(\gamma - 1)u]$[12]. These eigenvalues mean that the pressure vector $\mathbf{F'^p}$ only has down wind propagation, which does not reflect the true wave propagation and the vector is hence not strictly the wave vector. Most of the H-CUSP schemes such as the AUSM family schemes of Liou[3, 4, 5, 6, 7] average the pressure term $\mathbf{F'^p}$ in both upwind and downwind direction with the weight of $u \pm a$. Obviously, this is not consistent with the characteristics of $\mathbf{F'^p}$, which only has the downwind direction. Even though the upwinding treatment of the vector $\mathbf{F'^c}$ is justified according to its eigenvalues, the vector is not strictly the convective vector due to absorbing the pressure term in the energy equation.

2.3 The New E-CUSP Scheme

The new scheme is to develop a E-CUSP scheme that is consistent with the characteristic directions. Based on the characteristics of the vector $\mathbf{F^c}$ and $\mathbf{F^p}$, Zha and Bilgen suggested a simple flux vector splitting scheme as the following at subsonic regime[14]:

$$\mathbf{F}_{\frac{1}{2}} = \frac{1}{2}[\mathbf{F^c}_L + \mathbf{F^c}_R] - \frac{1}{2}[(|u|\mathbf{Q})_R - (|u|\mathbf{Q})_L]$$
$$+\frac{1}{2}[\begin{pmatrix} 0 \\ p(1+M) \\ p(u+a) \end{pmatrix}_L + \begin{pmatrix} 0 \\ p(1-M) \\ p(u-a) \end{pmatrix}_R]. \tag{12}$$

For supersonic flow, it switches to fully upwind scheme.

This scheme treats the convective vector $\mathbf{F^c}$ in an upwind manner and the pressure vector $\mathbf{F^p}$ with the eigenvalue $u \pm a$ weighted average from both the upwind and downwind directions. The pressure vector naturally transits to fully upwind in the supersonic regime. Most of the numerical dissipation terms of this scheme vanishes with the velocity approaching zero. By using the common interface speed of sound as suggested by Wada and Liou[4], the scheme can handle exact contact discontinuities[16]. However, due to lacking of the proper numerical dissipation, the scheme generates odd-even pressure oscillations when used for multi-dimensional flows.

To suppress the oscillations, the way to introduce the dissipation used by Wada and Liou for their AUSMD scheme [4] is borrowed to construct the convective term. First, the velocity u_L^+ and u_R^- are introduced as the following:

$$u_L^+ =$$
$$a_{\frac{1}{2}}\{\frac{M_L + |M_L|}{2} + \alpha_L[\frac{1}{4}(M_L+1)^2 - \frac{M_L + |M_L|}{2}]\} \tag{13}$$

$$u_R^- =$$
$$a_{\frac{1}{2}}\{\frac{M_R - |M_R|}{2} + \alpha_R[-\frac{1}{4}(M_R-1)^2 - \frac{M_R - |M_R|}{2}]\} \tag{14}$$

where the interface speed of sound $a_{\frac{1}{2}}$, Mach number, and α are evaluated as:

$$a_{\frac{1}{2}} = \frac{1}{2}(a_L + a_R) \tag{15}$$

$$M_L = \frac{u_L}{a_{\frac{1}{2}}}, \qquad M_R = \frac{u_R}{a_{\frac{1}{2}}} \tag{16}$$

$$\alpha_L = \frac{2(p/\rho)_L}{(p/\rho)_L + (p/\rho)_R}, \qquad \alpha_R = \frac{2(p/\rho)_R}{(p/\rho)_L + (p/\rho)_R} \tag{17}$$

An interface mass flux is introduced as the following:

$$(\rho u)_{\frac{1}{2}} = (\rho_L u_L^+ + \rho_R u_R^-) \tag{18}$$

Then the convective vector $\mathbf{F^c}$ is evaluated as:

$$\mathbf{F^c} = \frac{1}{2}[(\rho u)_{\frac{1}{2}}(\mathbf{q^c}_L + \mathbf{q^c}_R) - |\rho u|_{\frac{1}{2}}(\mathbf{q^c}_R - \mathbf{q^c}_L)] \tag{19}$$

where

$$\mathbf{q^c} = \begin{pmatrix} 1 \\ u \\ e \end{pmatrix} \tag{20}$$

The pressure term in the momentum equation uses the pressure splitting formulations of AUSM$^+$[5].

$$p_{\frac{1}{2}} = (\mathcal{P}^+ p)_L + (\mathcal{P}^- p)_R \tag{21}$$

where

$$\mathcal{P}^{\pm} = \frac{1}{4}(M \pm 1)^2(2 \mp M) \pm \alpha M(M^2-1)^2, \qquad \alpha = \frac{3}{16} \tag{22}$$

The pressure splitting in the energy equation uses the simple linear eigenvalues weighted average:

$$(pu)_{\frac{1}{2}} = \frac{1}{2}[p(u + a_{\frac{1}{2}})]_L + \frac{1}{2}[p(u - a_{\frac{1}{2}})]_R \qquad (23)$$

The energy pressure term may also use the higher order polynomial such as the Van Leer's Mach number splitting

$$(pu)_{\frac{1}{2}} = \frac{1}{4}a_{\frac{1}{2}}[p(M+1)^2]_L - \frac{1}{4}a_{\frac{1}{2}}[p(M-1)^2]_R \quad (24)$$

However, the numerical experiments indicated that eq.(24) is less robust and may generate oscillatory solutions. Hence the linear pressure splitting of eq.(23) is adopted. The drawback of the linear pressure splitting of eq.(23) is that the first order derivative is not continuous at the sonic point similar to the Steger-Warming scheme[17]. This may cause some non-smoothness at the sonic point when first order scheme is used. When higher than first order scheme is used, the non-smoothness disappears[16].

In summary, the new E-CUSP scheme can be written as the following:

For $|u| \le a$,

$$\mathbf{F}_{\frac{1}{2}} = \frac{1}{2}[(\rho u)_{\frac{1}{2}}(\mathbf{q^c}_L + \mathbf{q^c}_R) - |\rho u|_{\frac{1}{2}}(\mathbf{q^c}_R - \mathbf{q^c}_L)] + \begin{pmatrix} 0 \\ \mathcal{P}^+ p \\ \frac{1}{2}p(u + a_{\frac{1}{2}}) \end{pmatrix}_L + \begin{pmatrix} 0 \\ \mathcal{P}^- p \\ \frac{1}{2}p(u - a_{\frac{1}{2}}) \end{pmatrix}_R \qquad (25)$$

For $u > a$, $\mathbf{F}_{\frac{1}{2}} = \mathbf{F}_L$; For $u < -a$, $\mathbf{F}_{\frac{1}{2}} = \mathbf{F}_R$

where the definitions of the different terms are given as the following: eq.(18) for $(\rho u)_{\frac{1}{2}}$, eq.(20) for $\mathbf{q^c}$, eq.(22) for $\mathcal{P}^{\pm}$, eq.(15) for $a_{\frac{1}{2}}$, and eq.(16) for Mach number. The definitions of the Mach number and the interface speed of sound are essential to capture the exact contact discontinuities.

3 Numerical Dissipation

The low numerical dissipation at stagnation is important to accurately resolve wall boundary layers. The Liou's AUSM$^+$ scheme has all the numerical dissipation terms vanishing when the velocity approaches zero, which hence yields low numerical dissipation for wall boundary layers. For the new E-CUSP scheme, almost all of the numerical dissipation terms vanish with the velocity approaching zero, except one term in the energy equation due to the pressure splitting, eq.(23).

Assuming $u = 0$, the numerical dissipation vector of the new E-CUSP scheme at stagnation is:

$$\mathbf{D} = -\frac{a_{\frac{1}{2}}}{2}\begin{pmatrix} 0 \\ 0 \\ \delta p \end{pmatrix} \qquad (26)$$

where

$$\delta p = p_R - p_L \qquad (27)$$

The numerical dissipation of the Roe scheme at stagnation is:

$$\mathbf{D}_{Roe} = -\frac{\tilde{a}_{\frac{1}{2}}}{2(\gamma-1)}\begin{pmatrix} (\gamma-1)/\tilde{a}^2_{\frac{1}{2}}\delta p \\ 0 \\ \delta p \end{pmatrix} \qquad (28)$$

where the $\tilde{}$ stands for the Roe's average[2].

Comparing eq.(26) and (28), it can be seen that the numerical dissipation of the new E-CUSP scheme for the continuity equation vanishes at $u = 0$ while the Roe scheme has the non-vanishing dissipation. For the energy equation, the two schemes have equivalent dissipation. For ideal gas with the $\gamma = 1.4$, the coefficient of the Roe scheme energy dissipation term is 2.5 times larger than that of the new E-CUSP scheme.

In conclusion, even though there is one non-vanishing numerical dissipation term in the energy equation for the new E-CUSP scheme, the overall numerical dissipation of the new E-CUSP scheme is not greater than that of the Roe scheme. The Roe scheme is proved to be accurate to resolve wall boundary layers[18]. It is hence expected that the new E-CUSP scheme should also have sufficiently low dissipation to accurately resolve wall boundary layers. This is indeed the case shown by the numerical experiment for a flat plate boundary layer.

4 Extension to Multi-Dimensions

The 3D Navier-Stokes equations in conservation law form and in generalized coordinates is given as,

$$\frac{\partial \mathbf{Q}'}{\partial t} + \frac{\partial \mathbf{E}'}{\partial \xi} + \frac{\partial \mathbf{F}'}{\partial \eta} + \frac{\partial \mathbf{G}'}{\partial \zeta} = \frac{\partial \mathbf{R}'}{\partial \xi} + \frac{\partial \mathbf{S}'}{\partial \eta} + \frac{\partial \mathbf{T}'}{\partial \zeta} \quad (29)$$

Where Q' is the conservative variable vector, $\mathbf{E}', \mathbf{F}', \mathbf{G}'$ are the inviscid flux vectors in ξ, η, ζ directions, and $\mathbf{R}', \mathbf{S}', \mathbf{T}'$ are the viscous flux vectors in ξ, η, ζ directions, which are determined by the Reynolds average process to model the turbulence. To save the space,

the contents of the viscous fluxes will not be given here and can be found in the standard CFD text books.

$\mathbf{Q}'$ and $\mathbf{E}'$ are given below:

$$\mathbf{Q}' = \frac{1}{J}\begin{pmatrix} \rho \\ \rho u \\ \rho v \\ \rho w \\ \rho e \end{pmatrix}, \quad \mathbf{E}' = \begin{pmatrix} \rho U \\ \rho u U + l_x p \\ \rho v U + l_y p \\ \rho w U + l_z p \\ (\rho e + p) U \end{pmatrix} \tag{30}$$

Where J is the transformation Jacobian, u, v, w are the velocity components in x, y, z direction, U is the normal contravariant velocity in ξ direction:

$$U = \mathbf{V} \cdot \mathbf{l} = u l_x + v l_y + w l_z \tag{31}$$

The vector $\mathbf{l}$ is the control volume interface area vector pointing in the direction normal to the interface with the magnitude equal to the interface area. Let $\Delta\xi = \Delta\eta = \Delta\zeta = 1$ and then $\mathbf{l}$ is expressed as the following:

$$\mathbf{l} = l_x\mathbf{i} + l_y\mathbf{j} + l_z\mathbf{k} = \frac{1}{J}(\xi_x\mathbf{i} + \xi_y\mathbf{j} + \xi_z\mathbf{k}) \tag{32}$$

The flux of $\mathbf{F}'$ and $\mathbf{G}'$ can be obtained similarly following the symmetric rule in η and ζ direction.

When the control volume method is used, the discretized governing equation (29) can be rewritten as the following integral form,

$$\begin{aligned} &\frac{\partial}{\partial t}\int \mathbf{Q}' d\xi d\eta d\zeta + (\mathbf{E}'_{i+1/2} - \mathbf{E}'_{i-1/2}) \\ &+(\mathbf{F}'_{j+1/2} - \mathbf{F}'_{j-1/2}) + (\mathbf{G}'_{k+1/2} - \mathbf{G}'_{k-1/2}) = \\ &(\mathbf{R}'_{i+1/2} - \mathbf{R}'_{i-1/2}) + (\mathbf{S}'_{j+1/2} - \mathbf{S}'_{j-1/2}) \\ &+(\mathbf{T}'_{k+1/2} - \mathbf{T}'_{k-1/2}) \end{aligned} \tag{33}$$

Using the new CUSP scheme, the interface flux $\mathbf{E}'_{\frac{1}{2}}$ is evaluated as the following:

For $|U| \le a$,

$$\begin{aligned} \mathbf{E}'_{\frac{1}{2}} &= \frac{1}{2}[(\rho U)_{\frac{1}{2}}(\mathbf{q^c}_L + \mathbf{q^c}_R) - |\rho U|_{\frac{1}{2}}(\mathbf{q^c}_R - \mathbf{q^c}_L)] \\ &+ \begin{pmatrix} 0 \\ \mathcal{P}^+ p l_x \\ \mathcal{P}^+ p l_y \\ \mathcal{P}^+ p l_z \\ \frac{1}{2}p(U + a_{\frac{1}{2}}) \end{pmatrix}_L + \begin{pmatrix} 0 \\ \mathcal{P}^- p l_x \\ \mathcal{P}^- p l_y \\ \mathcal{P}^- p l_z \\ \frac{1}{2}p(U - a_{\frac{1}{2}}) \end{pmatrix}_R \end{aligned} \tag{34}$$

For $U > a$, $\mathbf{E}'_{\frac{1}{2}} = \mathbf{E}'_L$; For $U < -a$, $\mathbf{E}'_{\frac{1}{2}} = \mathbf{E}'_R$

where,

$$\mathbf{q^c} = \begin{pmatrix} 1 \\ u \\ v \\ w \\ e \end{pmatrix} \tag{35}$$

$(\rho U)_{\frac{1}{2}}$ and $\mathcal{P}^{\pm}$ are evaluated using eq.(13)-(18) and eq.(22) with u replaced by U.

Equation (3) is updated to include velocity u, v, w,

$$p = (\gamma - 1)[\rho e - \frac{1}{2}\rho(u^2 + v^2 + w^2)] \tag{36}$$

5 Results and Discussion

The new E-CUSP scheme will be compared with several other popularly used upwind schemes to study its performance. According to Godunov[19], when there are discontinuities in the solutions, monotone behavior of a solution can not be assured for finite difference method with higher than first order accuracy. Hence, for an upwind scheme to be used as a Riemann solver, it is essential to examine the performance of the scheme using first order accuracy. For the following test cases, all the 1D cases and the 2D flat plate laminar boundary layer use 1st order accuracy. The transonic nozzle and inlet-diffuser use 3rd order accuracy for the inviscid fluxes with MUSCL-type differencing[20] and the Minmod limiter.

5.1 Shock Tubes

For shock tube problems, the interests are focused on: 1) the quality (monotonicity and sharpness) of the shock and contact discontinuities; 2)the maximum allowable CFL number to be used for explicit Euler method.

For explicit Euler time marching scheme, it is desirable that the CFL number is close to the upper limit of 1.0. For the 1D linear wave equation with CFL=1 and 1st order upwind scheme, the numerical dissipation and dispersion vanish. For nonlinear Euler equations, it is also true that the closer the CFL to 1.0, the less the numerical dissipation.

5.1.1 The Sod Problem

Fig. 1 to 5 are the computed temperature distributions using different upwind schemes with first order accuracy compared with the analytical result of the Sod problem[21]. Since the computation stops before the

waves reach either end of the shock tube, the first order extrapolation boundary conditions are used at both ends of the shock tube for all the schemes.

The maximum allowable CFL number for a scheme is defined as: beyond which the solution will either be oscillatory or unstable. The new E-CUSP scheme (Zha CUSP in the figures) achieves maximum CFL of 1.00, and the shock profile is the crispest and remains monotone (Fig.1). The maximum allowable CFL of Roe and Van Leer scheme are 0.95 and 0.96 respectively. The new E-CUSP scheme takes three grid points across the shock wave, while the Roe and Van Leer schemes take four grid points (see Fig.1, 2 and 3). The Van Leer scheme generates a tail at the end of the expansion wave (see Fig. 3). Interestingly, the Van Leer-Hänel scheme can reach maximum CFL =1.0 and the shock profile is also crisper than the original Van Leer scheme with no tail generated at the end of the expansion wave (see Fig. 4). All the schemes smear the contact surface to a similar extent. The expansion wave is captured well by all the schemes. The AUSM$^+$ scheme has the unexpectedly low maximum allowable CFL of 0.275. The whole shock and contact surface profiles are seriously smeared due to the low maximum CFL number.

The table 1 given below summarizes the maximum allowable CFL number for each scheme. Overall, for the Sod 1D shock tube problem, the new scheme suggested in this paper performs the best based on the shock sharpness, monotonicity, and stability.

Table 1: Maximum CFL Numbers for Sod 1D Shock Tube

Scheme	CFL Number
The new scheme (Zha CUSP)	1.00
Van Leer-Hänel	1.00
Van Leer	0.96
Roe	0.95
Liou $AUSM^+$	0.275

5.1.2 Slowly Moving Contact Surface

This is a shock tube case used in [4] to demonstrate the capability of the scheme to capture the contact surface. The initial conditions are $[\rho, u, p]_L = [0.125, 0.112, 1.0]$, $[\rho, u, p]_R = [10.0, 0.112, 1.0]$. All the results are first order accuracy. Fig. 6 shows that the new E-CUSP scheme , the Roe scheme and the AUSM$^+$ scheme all can resolve the contact surface accurately as they are designed. The results of those schemes are at time level 0.01. The velocity is uniformly constant and the density discontinuity is monotone. The new E-CUSP (Zha CUSP) scheme has far higher CFL number than the other schemes with the value of 1.00. The Roe scheme has the max CFL=0.3, and Liou's AUSM$^+$ has 0.48. Fig.7 shows that the Roe scheme generates large velocity oscillations when CFL=0.35, greater than its max CFL=0.3.

The schemes of Van Leer, Van Leer-Hänel severely distort the profiles of the contact surfaces as shown in Fig. 8. The velocity profiles are largely oscillatory. The density jumps are also more smeared.

The table 2 lists the maximum CFL number of each scheme for the slowing moving contact surface. Again, the new scheme outperforms the other schemes by having the highest CFL number and still maintain the monotonicity.

Table 2: Maximum CFL numbers of the schemes resolving the contact surface

Scheme	CFL Number
The new E-CUSP (Zha CUSP) scheme	1.00
Liou $AUSM^+$	0.48
Roe	0.32
Van Leer	fail
Van Leer-Hänel	fail

5.2 Entropy condition

This case is to test if a scheme violates the entropy condition by allowing the expansion shocks. The test case is a simple quasi-1D converging-diverging transonic nozzle[15, 16]. The correct solution should be a smooth flow from subsonic to supersonic with no shock. However, for an upwind scheme which does not satisfy the entropy condition, an expansion shock may be produced.

For the subsonic boundary conditions at the entrance, the velocity is extrapolated from the inner domain and the other variables are determined by the total temperature and total pressure. For supersonic exit boundary conditions, all the variables are extrapolated from inside of the nozzle. The analytical solution was used as the initial flow field. Explicit Euler time marching scheme was used to seek the steady state solutions. All the schemes use first order differencing.

Fig. 9 is the comparison of the analytical and computed Mach number distributions with 201 mesh points using the new scheme and the scheme of Roe, Van Leer, Van Leer-Hänel, Liou's AUSM$^+$. The analytical solution is smooth throughout the nozzle and reaches the sonic speed at the throat (the minimum area of the nozzle, located at $X/h = 4.22$). It is seen that both the

Roe scheme and Van Leer scheme generate a strong expansion shock at the nozzle throat. Both schemes can converge to machine zero (12 order of magnitude) with CFL=0.95 even with the expansion shock waves.

The Van Leer-Hänel scheme can not converge even with CFL=0.01. The result plotted in Fig. 9 is the one before it diverges. It shows an expansion shock with the Mach number jumping from 0.74 to 1.42. The AUSM$^+$ also has difficulties to converge for this case. Using CFL=0.05, it managed to reduce the residual by 4 order of magnitude. The solution of the AUSM$^+$ also shows an expansion shock with the Mach number jumping from 0.86 to 1.17.

The new E-CUSP scheme does not have an expansion shock wave at the sonic point, but is not smooth due to the discontinuity of the first derivative of the pressure at the sonic point. This is shown as a small glitch at the sonic point in fig. 9. The glitch does not affect the scheme to converge the solution to machine zero with CFL=0.95.

As indicated in [15, 16], the amplitude of the expansion shock decreases when the mesh is refined. When the 2nd order schemes with the MUSCL differencing are used, all the expansion shock waves as well as the glitch of the new scheme at the sonic point disappear. Since this paper is to compare the original Riemann solver schemes, no entropy fix[22] that can remove the expansion shock of Roe schemes was used.

5.3 Wall Boundary Layer

To examine the numerical dissipation of the new scheme, a laminar supersonic boundary layer on an adiabatic flat plate is calculated using first order accuracy. The incoming Mach number is 2.0. The Reynolds number based on the length of the flat plate is 40000. The Prandtl number of 1.0 is used in order to compare the numerical solutions with the analytical solution. The baseline mesh size is 81×61 in the direction along the plate and normal to the plate respectively.

Fig.10 is the comparison between the computed velocity profiles and the Blasius solution. The solutions of the new scheme (Zha CUSP), Roe scheme, and AUSM$^+$ scheme agree very well with the analytical solution. The Van Leer scheme significantly thickens the boundary layer. The Van Leer- Hänel scheme does not improve the velocity profile.

Fig.11 is the comparison between the computed temperature profiles and the Blasius solution. Again, the new scheme (Zha CUSP), Roe scheme, and AUSM$^+$ scheme accurately predict the temperature profiles and the computed solutions basically go through the analytical solution. Both the Van Leer scheme and the Van Leer- Hänel scheme significantly thicken the thermal boundary layer similarly to the velocity profiles.

Table 3 shows the wall temperature predicted by all the schemes using the baseline mesh and refined mesh. The predicted temperature value by the Van Leer scheme has a large error. The Van Leer- Hänel scheme does predict the wall temperature accurately even though the overall profile is nearly as poor as that predicted by the Van Leer scheme. The new scheme, Roe scheme and AUSM+ scheme all predict the temperature accurately.

All the results mentioned above are converged based on mesh size. The wall temperatures using the refined mesh of 161×121 are also given in table 3. There is little difference between the results of the baseline mesh and the refined mesh. The refined mesh does not help to reduce the large numerical dissipation of the Van Leer scheme. When the 2nd order schemes are used, both the velocity and temperature profiles of the Van Leer scheme and Van Leer- Hänel are improved (not shown).

Scheme	T_{wall}, baseline	T_{wall}, refined
Blasius	1.8000	1.8000
new scheme	1.8025	1.8018
Roe scheme	1.8002	1.7996
Liou $AUSM^+$	1.8000	1.8000
Van Leer	1.8328	1.8333
Van Leer-Hänel	1.7970	1.7996

Table 3: Computed non-dimensional wall temperature using first order schemes with the baseline mesh and refined mesh

5.4 Transonic Converging-Diverging Nozzle

To examine the performance of the new scheme in two-dimensional flow and the capability to capture the shock waves which do not align with the mesh lines, a transonic converging-diverging nozzle is calculated as inviscid flow. The nozzle was designed and tested at NASA and was named as Nozzle A1[23]. Third order accuracy of MUSCL type differencing is used to evaluate the inviscid flux with the Minmod limiter. Fig.12 is the computed Mach number contour using the new E-CUSP scheme with the mesh size of 175×80. In the axial direction, there are 140 mesh points distributed downstream of the nozzle throat, where the oblique shock waves are located. The grid is clustered near the wall. For clarity, the coarsened mesh is drawn as the background with the Mach contours to show the relative orientation of the shock waves and the mesh lines. The nozzle is symmetric about the centerline. Hence only upper half of the nozzle is calculated. The

upper boundary uses the slip wall boundary conditions and the lower boundary of the center line uses the symmetric boundary conditions.

As indicated by the wall surface isentropic Mach number distribution shown in fig.13, the flow is subsonic at the inlet with the Mach number about 0.22 and is accelerated to sonic at the throat, and then reaches supersonic with Mach number about 1.35 at the exit. Fig.12 shows that right after throat, an expansion fan emanates from the wall and accelerates the flow to reach the peak Mach number about 1.5. Due to the sharp throat turning, an oblique shock appears immediately downstream of the expansion fan to turn the flow to axial direction. The two oblique shocks intersect at the centerline, go through each other, hit the wall on the other side, and then reflect from the wall. Such shock patten is repeated to the exit and the shock strength is weakened with the flow going downstream. Fig. 13 shows that the isentropic Mach number distributions predicted by the new CUSP scheme and the Roe scheme agree fairly well with the experiment. The new E-CUSP scheme and the Roe scheme have virtually indistinguishable results.

The mesh refinement study indicates that the mesh resolution in the axial direction does not affect the shock resolution much. The axial mesh size of 280 downstream of the throat yields only slightly better shock resolution than the size of 70. However, the mesh size in the vertical direction dramatically changes the shock resolution. The mesh size of 80 in the vertical direction yields much better resolution than the mesh size of 50. This can be seen from the isentropic Mach number in fig.13, which shows that the mesh size of 175×80 generates much sharper profiles than those of the mesh 175×50 for the first and second shock reflections.

For this transonic nozzle with the mesh size 175×80 on an Intel Xeon 1.7Ghz processor, the CPU time per time step per node to calculate the inviscid flux is $2.5871 \times 10^{-6} s$ for the new scheme, which is about 25% of the CPU time of $1.0284 \times 10^{-5} s$ used for the Roe scheme. This is a significant CPU time reduction.

5.5 Transonic Inlet-Diffuser

To examine the performance of the new scheme for shock wave/turbulent boundary layer interaction, a transonic inlet-diffuser[24] is calculated as shown by the Mach number contours in fig.14, which has the exit back pressure equal to 0.83 times of the inlet total pressure. The Reynolds number based on the throat height is 4.38×10^5. The Baldwin-Lomax[25] algebraic turbulence model is used. Third order accuracy of MUSCL-type differencing with the Minmod limiter is used for the inviscid fluxes and the second order central differencing is used for the viscous terms.

A normal shock is located downstream of the throat as shown in fig.14. No flow separation is generated under this back pressure. The baseline mesh size is 100×60. When y_1^+ is held as constant and the mesh is refined in both the horizontal and vertical direction, the results have little variation and are converged based on mesh size. All the inlet-diffuser results presented in this paper are from the mesh size of 100×120. The mesh in the horizontal direction is clustered around the shock location to better resolve the shock profile.

Fig. 15 is the comparison of the upper wall surface pressure between the experiment and the computation. The agreement is very good except that the computation predicts the shock location a little downstream of the experimental shock location and the shock strength a little too strong. It is found that the shock profile is sensitive to the y_1^+. The y_1^+ value of $2, 2 \times 10^{-4}, 7 \times 10^{-6}$ are tested. The smaller y_1^+ yields a little closer shock location to the experiment. The results shown in fig.14 and 15 have the y_1^+ value of 2×10^{-4}. The small y_1^+ effect is believed due to the first order extrapolation of the pressure on wall surface instead of the requirement of the turbulence modeling. In the region with no shock, the first order pressure extrapolation on the wall is insensitive to the distance of the first cell to the wall, while in the shock region it is sensitive due to the large streamwise gradient. As indicated in fig. 15, the Roe scheme predicts the shock location slightly closer to the experiment than the new CUSP scheme.

When the back pressure is reduced to 0.72 times of the inlet total pressure. The normal shock is stronger and the flow separation is induced. The same mesh as the previous case is used for this case. Fig.17 is the predicted pressure distribution compared with the experiment. Both the new CUSP scheme and the Roe scheme predict the shock location accurately, but the shock strength predicted is too strong. However, the new scheme has the pressure profile in the separation region downstream of the shock noticeably closer to the experiment than that predicted by the Roe scheme.

It should be pointed out that the turbulence modeling is a critical factor for the prediction accuracy of the shock wave/turbulent boundary layer interaction. Hence the discrepancy between the calculation and experiment shown above is only partially attributed to the different discretization schemes.

Fig.17 is the pressure contours computed using $p_{out}/p_t = 0.72$ with the new scheme, Roe Scheme, and Liou's AUSM$^+$ scheme. A curved λ shock is formed due to the shock wave/turbulent boundary layer interaction. The shape of the Mach contours of the new scheme (Zha CUSP) and the Roe scheme are very much alike. The contours computed by the AUSM$^+$ scheme

has significant oscillations near the wall.

6 Conclusions

A new efficient upwind scheme based on the concept of convective upwind and split pressure (CUSP) is developed. The upwinding of the convective term and the pressure splitting are consistent with their characteristics directions. The numerical dissipation of the new scheme at stagnation is low and is not greater than that of the Roe scheme. The scheme hence is able to resolve accurately wall boundary layers, and are able to capture crisp shock waves and exact contact discontinuities. The performance of the new scheme is compared with the Roe scheme, AUSM$^+$ scheme, Van Leer scheme, and Van Leer-Hänel scheme.

For the 1D Sod shock tube problem using Euler explicit scheme, the new scheme has the crispest shock profile and highest allowable CFL number of 1.0. For a slowly moving contact surface, the new scheme is demonstrated to capture the exact contact surface discontinuity with the maximum allowable CFL of 1.0, which is far greater than that of the other schemes. For a quasi-1D transonic nozzle, all the other schemes generate expansion shocks at the sonic point. The new scheme does not have the expansion shock even though it has a glitch at the sonic point, which is due to the discontinuity of the first derivative of the pressure splitting at sonic point.

For a Mach=2.0 supersonic adiabatic laminar flat plate boundary layer, the new scheme is able to accurately resolve the boundary layer velocity and temperature profiles using the first order differencing. The solution is as accurate as that of the Roe scheme and the AUSM$^+$ scheme and hence demonstrates the low diffusion of the new scheme.

For a transonic converging-diverging nozzle, oblique shock waves and reflections are crisply captured even though the shock waves do not align with the mesh lines. The predicted wall surface isentropic Mach number distribution agrees well with the experiment. For a transonic inlet-diffuser with shock/turbulent boundary layer interaction, the new scheme and the Roe scheme predict the surface pressure distributions agreeing well with the experiment for the case of a weak shock. For the strong shock case, both the new scheme and the Roe scheme over predict the strength of the shock wave. However, the pressure distribution predicted by the new scheme is closer to the experiment. The AUSM$^+$ solution has large pressure oscillations.

In conclusion, the new scheme is proved to be accurate, robust and efficient for the flow cases tested in this paper.

7 Acknowledgment

This work is partially supported by AFOSR Grant F49620-03-1-0253 monitored by Major William Hilbun.

References

[1] P. Roe, "CFD Algorithms." NASA Spring Workshop on Fluids, University of Alabama, Birmingham, Alabama, USA, April 22-24, 2003.

[2] P. Roe, "Approximate Riemann Solvers, Parameter Vectors, and Difference Schemes," *Journal of Computational Physics*, vol. 43, pp. 357–372, 1981.

[3] M.-S. Liou and C. J. Steffen, "A New Flux Splitting Scheme," *Journal of Computational Physics*, vol. 107, pp. 1–23, 1993.

[4] Y. Wada and M.-S. Liou, "An Accurate and Robust Splitting Scheme for Shock and Contact Discontinuities." AIAA Paper 94-0083, 1994.

[5] M.-S. Liou, "Progress Towards an Improved CFD Methods: AUSM$^+$." AIAA Paper 95-1701-CP, June, 1995.

[6] M.-S. Liou, "A Sequel to AUSM: AUSM$^+$," *Journal of Computational Physics*, vol. 129, pp. 364–382, 1996.

[7] M.-S. Liou, "Ten Years in the Making-AUSM-Family." AIAA 2001-2521, 2001.

[8] D. Hänel, R. Schwane, and G. Seider, "On the Accuracy of Upwind Schemes for the Solution of the Navier-Stokes Eqautions." AIAA paper 87-1105 CP, 1987.

[9] J. R. Edwards, "A Low-Diffusion Flux-Splitting Scheme for Navier-Stokes Calculations." AIAA Paper 95-1703-CP, June, 1995.

[10] J. R. Edwards, "A Low-Diffusion Flux-Splitting Scheme for Navier-Stokes Calculations," *Computer & Fluids*, vol. 6, pp. 635–659, 1997.

[11] A. Jameson, "Analysis and Design of Numerical Schemes for Gas Dynamics I: Artificial Diffusion, Upwind Biasing, Limiters and Their Effect on Accuracy and Multigrid Convergence in Transonic and Hypersonic Flow." AIAA Paper 93-3359, July, 1993.

[12] A. Jameson, "Analysis and Design of Numerical Schemes for Gas Dynamics I: Artificial Diffusion, Upwind Biasing, Limiters and Their Effect on Accuracy and Multigrid Convergence in Transonic and Hypersonic Flow," *Journal of Computational Fluid Dynamics*, vol. 4, pp. 171–218, 1995.

[13] A. Jameson, "Analysis and Design of Numerical Schemes for Gas Dynamics II: Artificial Diffusion and Discrete Shock Structure," *Journal of Computational Fluid Dynamics*, vol. 5, pp. 1–38, 1995.

[14] G.-C. Zha and E. Bilgen, "Numerical Solutions of Euler Equations by Using a New Flux Vector Splitting Scheme ," *International Journal for Numerical Methods in Fluids*, vol. 17, pp. 115–144, 1993.

[15] G.-C. Zha, "Numerical Tests of Upwind Scheme Performance for Entropy Condition ," *AIAA Journal*, vol. 37, pp. 1005–1007, 1999.

[16] G.-C. Zha, "Comparative Study of Upwind Scheme Performance for Entropy Condition and Discontinuities." AIAA Paper 99-CP-3348, June 28- July 1, 1999.

[17] J. Steger and R. Warming, "Flux Vvector Splitting of the Inviscid Gasdynamic Equations with Application to Finite-Difference Methods," *Journal of Computational Physics*, vol. 40, pp. 263–293, 1981.

[18] B. Van Leer, J. Thomas, P. L. Roe, and R. Newsome, "A Comparison of Numerical Flux Formulas for the Euler and Navier-Stokes Equations." AIAA paper 87-1104, 1987.

[19] S. Godunov, "Finite-Difference Method for Numerical Computation of Discontinuous Solutions of the Equations of Fluid Dynamics," *Mat. Sb.*, vol. 47, pp. 271–306, 1959.

[20] B. Van Leer, "Towards the Ultimate Conservative Difference Scheme, III," *Journal of Computational Physics*, vol. 23, pp. 263–75, 1977.

[21] G. Sod, "A survey of several finite difference methods for systems of nonlinear hyperbolic conversation laws," *Journal of Computational Physics*, vol. 27, pp. 1–31, 1978.

[22] A. Harten, P. D. Lax, and B. Van Leer, "On Upstream Differencing and Godunov-type Scheme for Hyperbolic Conservation Laws," *SIAM Review*, vol. 25, No.1, pp. 35–61, Jan. 1983.

[23] M. L. Mason and L. E. Putnam, "The Effect of Throat Contouring on Two-Dimensional Converging-Diverging Nozzles at Static Conditions ." NASA Technical Paper 1704, 1980.

[24] T. Bogar, M. Sajben, and J. Kroutil, "Characteristic Frequency and Length Scales in Transonic Diffuser Flow Oscillations." AIAA Paper 81-1291, 1981.

[25] B. Baldwin and H. Lomax, "Thin Layer Approximation and Algebraic Model for Separated Turbulent Flows." AIAA Paper 78-257, 1978.

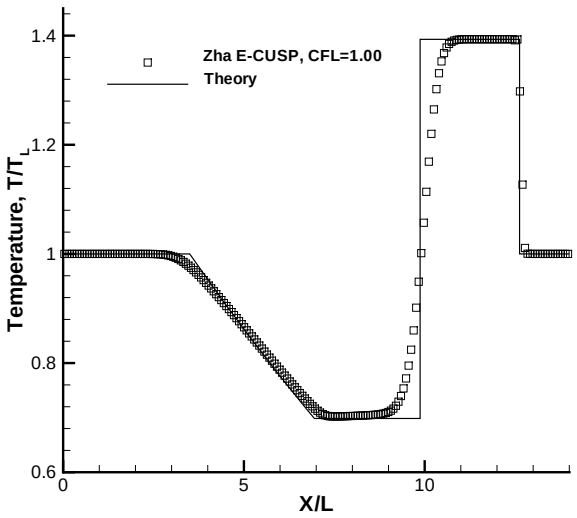

Figure 1: Temperature distribution of the Sod 1D shock tube computed by Zha E-CUSP scheme

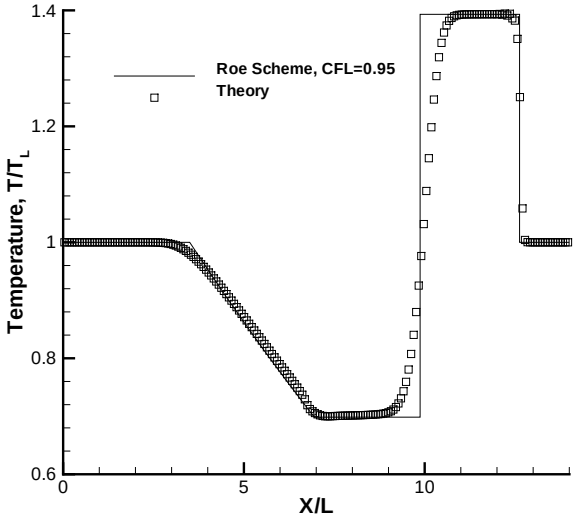

Figure 2: Temperature distribution of the Sod 1D shock tube computed by Roe scheme

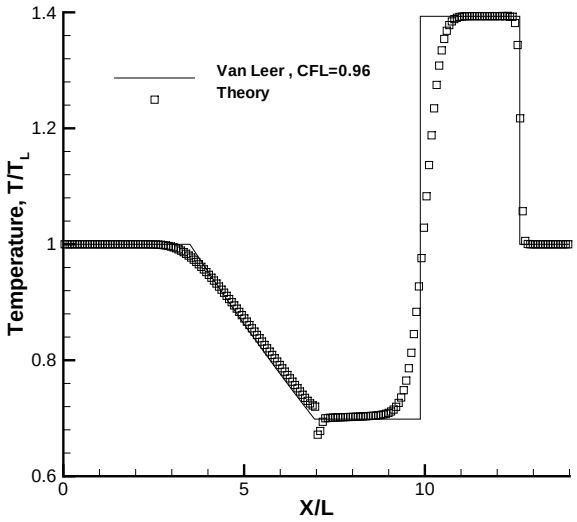

Figure 3: Temperature distribution of the Sod 1D shock tube computed by Van Leer scheme

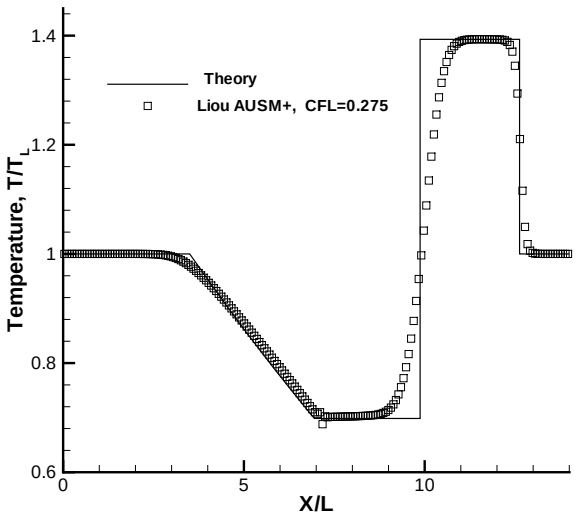

Figure 5: Temperature distribution of the Sod 1D shock tube computed by AUSM$^+$ scheme

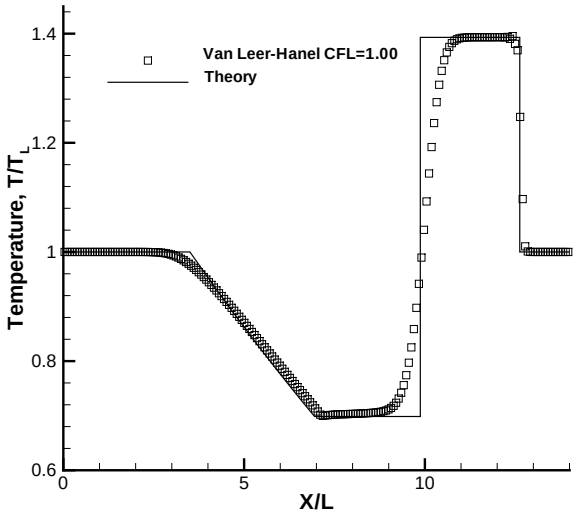

Figure 4: Temperature distribution of the Sod 1D shock tube computed by Van Leer-Hänel scheme

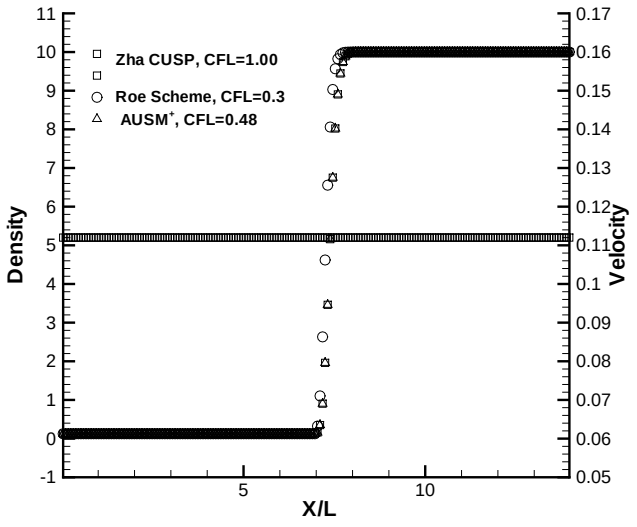

Figure 6: Computed density and velocity profiles of a slowly moving contact surface

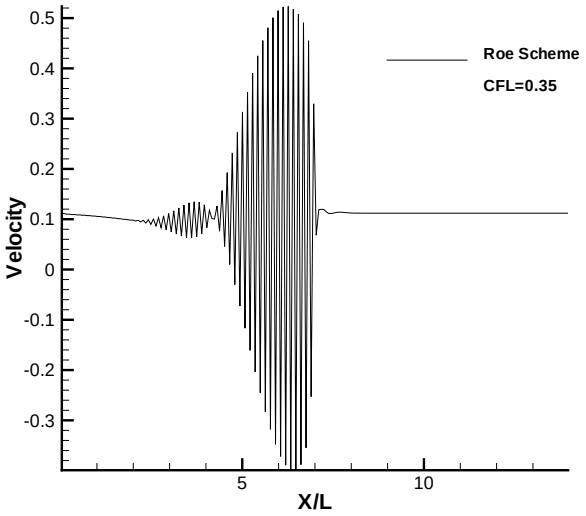

Figure 7: Computed density profile of a slowly moving contact surface using the Roe scheme

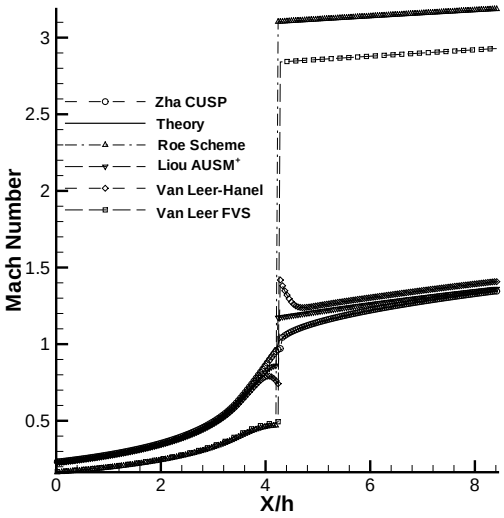

Figure 9: Computed Mach number distributions for the converging-diverging nozzle

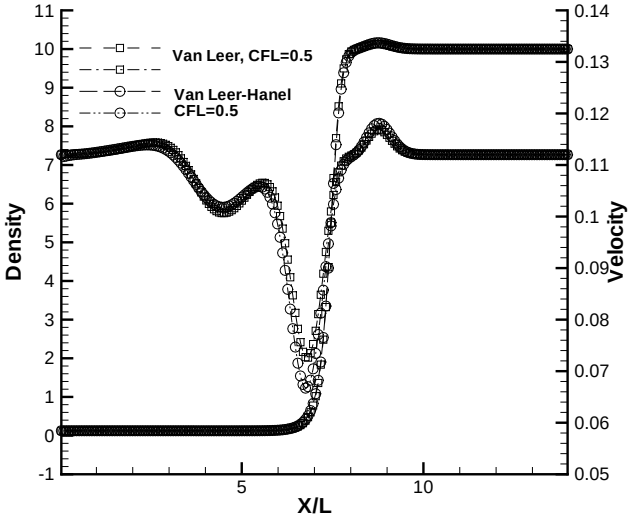

Figure 8: Computed density and velocity profiles of a slowly moving contact surface

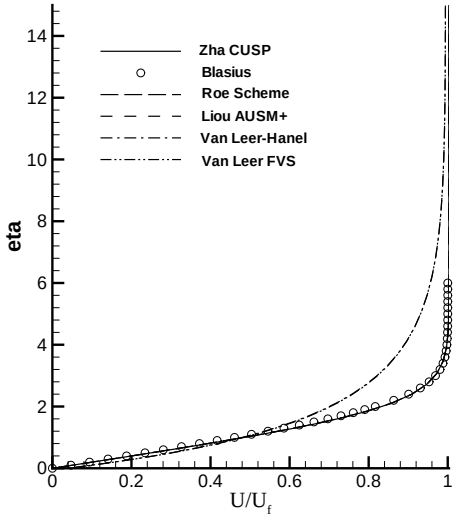

Figure 10: Computed velocity profiles of the laminar boundary layer using 1st order schemes

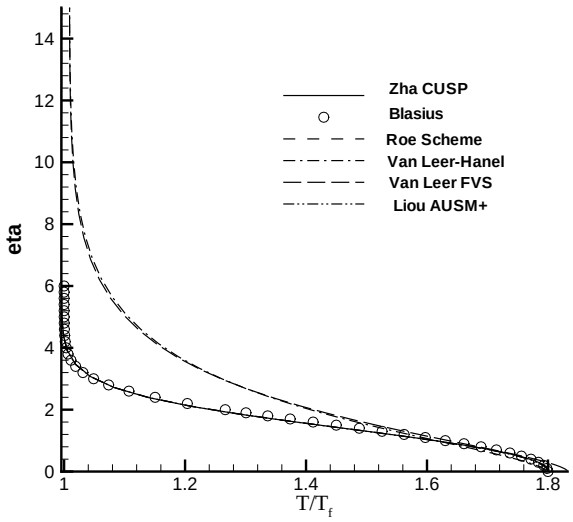

Figure 11: Computed temperature profiles of the laminar boundary layer using 1st order schemes

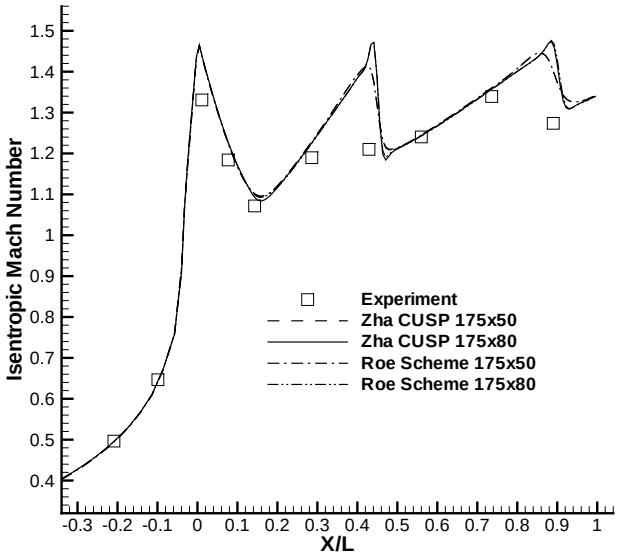

Figure 13: Adiabatic Mach number distribution computed on the wall surface of the nozzle

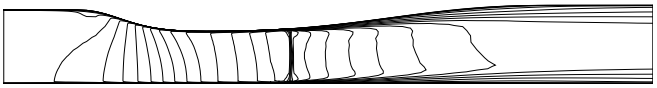

Figure 14: Computed Mach number contours using the Zha CUSP scheme with $p_{out}/p_t = .83$

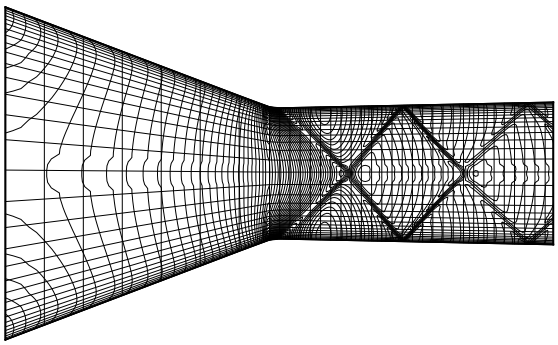

Figure 12: Computed Mach number contours using the Zha CUSP scheme

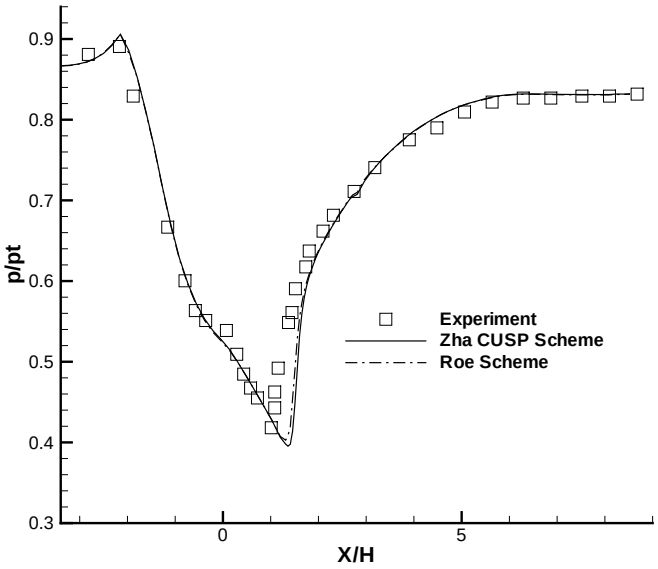

Figure 15: Static pressure distribution computed on the upper surface of the inlet-diffuser ($p_{out}/p_t = .83$)

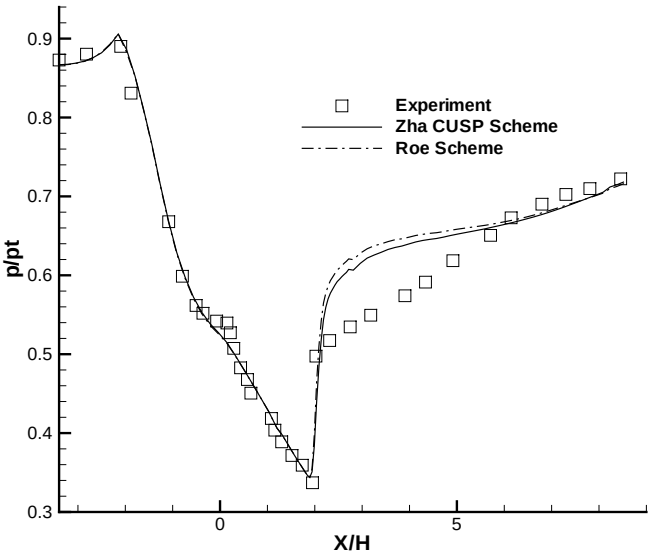

Figure 16: Static pressure distribution computed on the upper surface of the inlet-diffuser ($p_{out}/p_t = .72$)

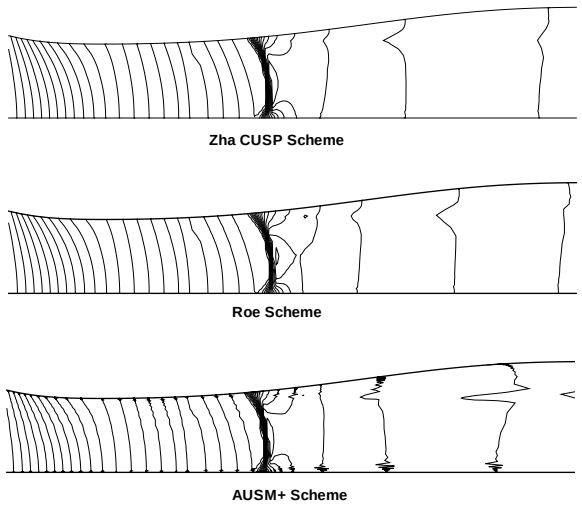

Figure 17: Comparison of computed pressure contours using the Zha CUSP scheme, Roe Scheme, and Liou's AUSM$^+$ scheme ($p_{out}/p_t = .72$)